Tonga Ridge and Lau Basin crustal structure from seismic refraction data

Wayne C. Crawford, John A. Hildebrand, Leroy M. Dorman, Spahr C. Webb, Douglas A. Wiens

Tonga Ridge and Lau Basin crustal structure from seismic refraction data

Wayne C. Crawford,[1] John A. Hildebrand, and LeRoy M. Dorman
Scripps Institution of Oceanography, La Jolla, California, USA

Spahr C. Webb
Lamont Doherty Earth Observatory, Palisades, New York, USA

Douglas A. Wiens
Washington University, St Louis, Missouri, USA

Received 2 October 2001; revised 31 May 2002; accepted 29 January 2003; published 11 April 2003.

[1] The crustal structure across the Tonga-Lau arc-back arc system from the Lau Ridge to the Pacific Plate (178°–170°W, 18°19°S) is modeled, using data from an 840-km-long air gun refraction line over 19 ocean bottom seismometers and one land station. The data reveal that the Pacific Plate crust is 5.5 km thick, with a velocity structure similar to that found at the present-day East Pacific Rise (EPR). Beneath Tonga Ridge, an intermediate velocity layer (6–7 km/s) is up to 7.5 km thick and has a velocity-depth distribution similar to andesitic rocks found in continental crust. The crust is abnormally thin (4 km) at the boundary between the Tonga Ridge and the Lau Basin. At the east end of Lau Basin, the crust is 5.5–6.5 km thick and resembles crust formed at the EPR except for a thicker sheeted-dike section (2–3 km) and thinner lower crust (2 km). The Lau Basin crust thickens to 7–8 km near the Central Lau Spreading Center (CLSC), mostly through thickening of the lower crust. The crust thickens again to 8.5–9.5 km at 50 km west of the CLSC, mostly through thickening of the midcrust. In the thick westernmost section, the crustal structure is uniform even though one part of this section formed through extension of arc-type crust while the rest was created at an oceanic spreading center. The relative homogeneity of these rocks suggests that their petrology may be dominated by postemplacement magmatic infilling from a mantle source west of the spreading center. *INDEX TERMS:* 3040 Marine Geology and Geophysics: Plate tectonics (8150, 8155, 8157, 8158); 3025 Marine Geology and Geophysics: Marine seismics (0935); 8150 Tectonophysics: Evolution of the Earth: Plate boundary—general (3040); *KEYWORDS:* Tonga, Lau, seismic refraction, island arc, back arc basin

Citation: Crawford, W. C., J. A. Hildebrand, L. M. Dorman, S. C. Webb, and D. A. Wiens, Tonga Ridge and Lau Basin crustal structure from seismic refraction data, *J. Geophys. Res.*, *108*(B4), 2195, doi:10.1029/2001JB001435, 2003.

1. Introduction

[2] The Tonga-Lau region is a compact microcosm of plate tectonics, containing zones of lithospheric subduction, island arc building, and oceanic crustal formation (Figure 1). The Pacific Plate subducts beneath the Indo-Australian plate at the Tonga Trench, and melt is believed to rise from the subducting slab to form the volcanic Tonga Ridge. Since at least 25 Ma, the Pacific Plate has moved away from the Indo-Australian plate, splitting the original volcanic ridge first by extension, then by seafloor spreading. The seafloor spreading started approximately 6 Ma at the north end of the Tonga-Lau region and has since propagated 700 km south to form the V-shaped Lau Basin.

[3] Lau Basin currently opens at two overlapping, southward propagating spreading centers. The spreading rate is comparable to that of the ''fast spreading'' East Pacific Rise (EPR) [*Bevis et al.*, 1995], making this basin a good place to test fast spreading accretion models, which for the most part are based on EPR studies. In fact, the Lau Basin crust is noticeably different than that created at the EPR. The Lau Basin seafloor is shallower (2–2.5 km versus 3–4 km) and the crust appears to be thicker than near the EPR (8–9 km versus 6–7 km [*Karig*, 1970; *White et al.*, 1992; *Turner et al.*, 1999]). The crustal melt lens beneath the Lau spreading center is also deeper than the EPR melt lens (2.2–3.5 km versus 1.4–1.8 km [*Collier and Sinha*, 1992; *Purdy et al.*, 1992; *Kent et al.*, 1993; *Turner et al.*, 1999]) except on part of the Central Lau Spreading Center (CLSC) where the melt lens may be as shallow as 1.1 km [*Harding et al.*, 2000]. Finally, most of the crustal thickness variations at the EPR come in the form of lower crustal (gabbro) variations [*Harding et al.*, 1993; *Barth and Mutter*, 1996], while

[1]Now at Laboratoire de Geosciences Marines, Institut de Physique du Globe de Paris, Paris.

0148-0227/03/2001JB001435$09.00

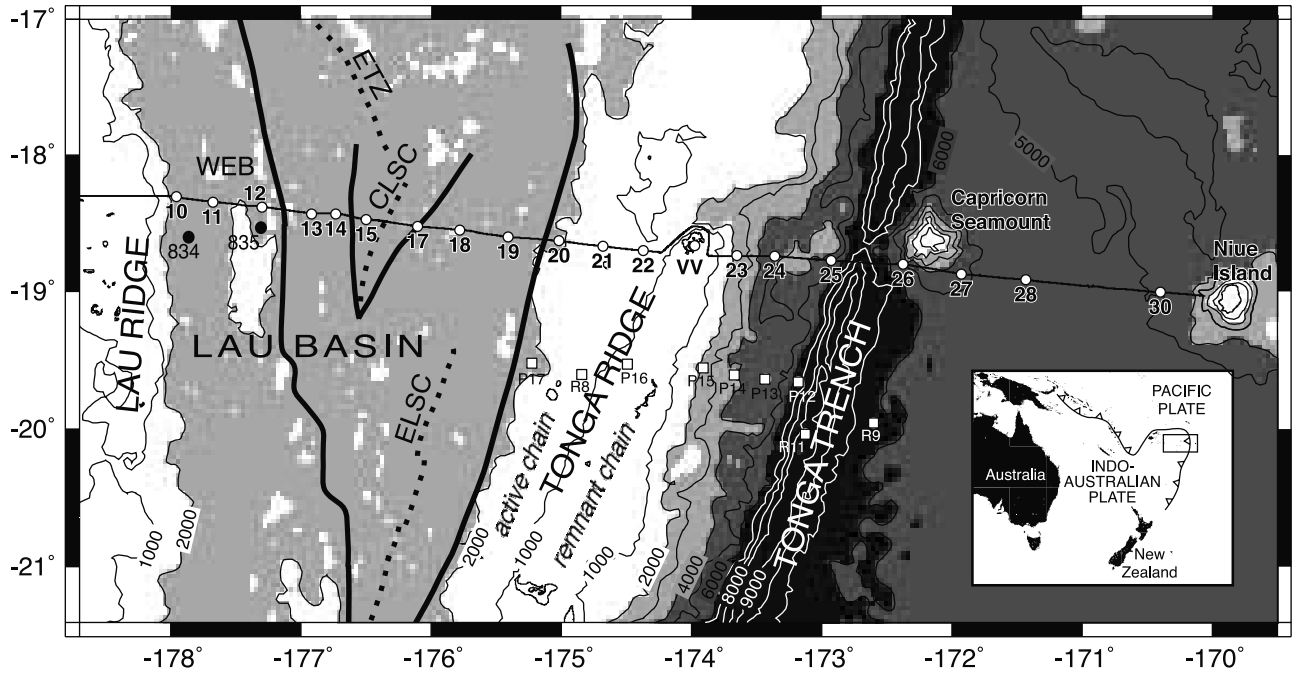

Figure 1. The regional setting with ocean bottom seismograph (OBS) and the land station (VV) marked by open circles and the air gun track indicated by the thin solid line connecting the circles. Dotted lines mark spreading centers and transforms. Bold solid lines mark estimated bounds of crust created at the spreading centers. Geological information compiled from *Parson and Hawkins* [1994], *Parson et al.* [1994], *Hawkins* [1995], and *Taylor et al.* [1996]. WEB indicates Western Extensional Basin, CLSC indicates Central Lau Spreading Center, ELSC indicates Eastern Lau Spreading Center, ETZ indicates Extensional transform zone, 834 and 835 indicate ODP drill holes. Open squares mark centerpoints of previous 1-D seismic surveys (R sites are from *Raitt et al.* [1955], P sites are from *Pontoise and Latham* [1982]).

midcrustal (sheeted dike) variations appear to play a more important role in Lau Basin [*Turner et al.*, 1999], perhaps indicating a more variable melt lens depth beneath the Lau spreading centers.

[4] These differences may arise in part from differences in the melt supply to the Lau Basin and the EPR. The source of mantle melt to Lau Basin appears to be centered west of the spreading centers and is relatively shallow. This melt supply may directly feed the western part of Lau basin as well as the spreading centers. Mid-ocean ridge basalt (MORB)-type basalts subsequently filled grabens in western Lau Basin, originally formed by extension of island arc rock. This asymmetric melt supply may continue today, as indicated by a low-velocity anomaly in the upper mantle teleseismically imaged beneath west Lau Basin [*Zhao et al.*, 1997; *Roth et al.*, 1999].

[5] The velocity structure of the Tonga Ridge crust may contain important information about how island arcs form. Island arcs have been implicated as the source of continental crust [e.g., *McLennan and Taylor*, 1982], and, since the bulk composition of continental crust is andesitic, the simplest form of this theory predicts that island arcs are also andesitic. However, dredging and drilling indicates that the bulk composition of island arcs may be closer to basalt, and only a few island arcs have been well studied seismically to determine deeper structure. Some of these contain a deep layer with velocities in the range 6–6.5 km/s, corresponding well to andesitic rocks in continental crust (e.g., Izu-Ogasawara [*Suyehiro et al.*, 1996]), while others contain no such layer (e.g., the Aleutian arc [*Holbrook et al.*, 1999]). More island arcs need to be studied to determine if andesitic rocks are often formed beneath island arcs and to identify the factors controlling their formation.

[6] In 1994 a research team from the Scripps Institution of Oceanography and Washington University deployed 30 ocean bottom seismographs (OBSs) across the Tonga-Lau region as part of an active and passive seismic imaging experiment. Nineteen of the OBSs were deployed on a line perpendicular to the regional structure to create a two-dimensional (2-D) cross section, and 11 OBSs were deployed off-line to reveal 3-D structure. The passive experiment was designed to listen to regional earthquakes and thus improve the resolution of regional mantle structure, while the active experiment was designed to constrain crustal structure.

[7] We report here the results of the active seismic experiment. We use 5148 air gun shots from the R/V *Melville* on an 840-km line crossing the 19 aligned OBSs and one island seismic station to construct a two-dimensional model of the crust from the Pacific Plate to the Lau Ridge. All of the seismometers recorded refractions in the crust from the air gun shots, and most of them recorded arrivals refracted in the upper mantle. We use a two-dimensional inverse code [*Zelt and Smith*, 1992] to fit the crustal

and mantle refractions and Moho reflections. We present the resulting model and discuss the implications of this model for the structure and genesis of Tonga-Lau crust.

2. Site Description

[8] The active seismic survey crosses the Tonga-Lau region at 18°–19°S, crossing Lau Basin, the CLSC, the Tonga Arc, the Tonga Trench, the southern end of Capricorn seamount, and 100 km of Pacific Plate (Figure 1). Within an Australian reference frame, the Lau Ridge and western Lau Basin are fixed, eastern Lau basin and the Tonga Ridge move ~130 mm/yr ESE, and the Pacific Plate moves ~75 mm/yr WNW [*Bevis et al.*, 1995].

[9] The Lau Basin comprises crust formed at two southward propagating spreading centers plus a 100-km-wide strip created by extension of the original island arc. The Eastern Lau Spreading Center (ELSC) started opening 4–6 Ma near 17°S and has since propagated 700 km south. The CLSC formed later, near 18°S and west of the ELSC, and is now the spreading center between 18° and 19.5°S. Seismic studies of the Valu Fa ridge at the south end of the ELSC reveal a 0.6- to 4-km-wide melt lens 2.9 ± 0.3 km beneath the seafloor, overlying an ~4-km-wide, 3-km-thick low velocity zone. There, the crust is 8–9 km thick within 60 km of the ridge [*Morton and Sleep*, 1985; *Collier and Sinha*, 1992; *Turner et al.*, 1999]. A recent seismic study of the northern ELSC and the CLSC reveals an axial melt lens 2–2.6 km beneath the seafloor at the north end of the ELSC and 1.1–1.6 km beneath the seafloor at the south end of the CLSC [*Harding et al.*, 2000].

[10] The Lau Basin is mostly floored by MORB-like rocks, but the westernmost 80–120 km is floored by a mixture of MORB, transitional, and arc-like basalts [*Hawkins*, 1995]. This western region, known as the Western Extensional Basin (WEB), is believed to have been formed by extension and rifting between the Lau and Tonga Ridges before seafloor spreading started, followed by infilling of the grabens by fresh magma from a mantle source that is chemically distinct from the CLSC/ELSC source [*Hawkins*, 1995].

[11] Earthquake tomography reveals a low-velocity zone centered in the upper 100 km of mantle west of the CLSC. The zone is centered ~50 km beneath the seafloor [*Xu and Wiens*, 1997; *Zhao et al.*, 1997; *Roth et al.*, 1999], shallower than the velocity minimum imaged elsewhere beneath oceanic spreading centers [e.g., *Zhang and Tanimoto*, 1992]. Near the base of the crust, *P*-wave *Q* is as low as 95, and *P*-wave velocity is as low as 7.6 km/s. *S*-wave velocity is 3.8 km/s in the center of the low-velocity zone.

[12] The Tonga Ridge contains an active and a remnant volcanic chain. The eastern, remnant chain contains the coral islands of the Tonga group and consists of uplifted carbonates and gravity flow sediment deposits overlying middle Eocene to late Miocene volcanic and plutonic rocks. The western, active Tofua chain formed 0–3 Ma and is made up of basaltic seamounts, shoals, and rocky islands. On the forearc to the east of the chains, Miocene sediments fault against flows, tuffs, and tuff breccias believed to have been part of a prior island arc [*Hawkins*, 1995]. Seismic studies image thick sediments on this forearc section and between the two island chains [*Raitt et al.*, 1955; *Karig*, 1970; *Pontoise and Latham*, 1982].

Table 1. Seismometer Positions, Sampling Rates, and Channels Used for Picking

Site Name	Latitude South	Longitude West	Depth, m	Rate, Hz	Channel Picked
S10	18°18.394	177°57.551	2565	32	P[a]
S11	18°20.684	177°40.429	2444	128	Z[b]
S12	18°22.832	177°18.047	2610	32	P
S13	18°25.812	176°55.219	2423	128	Z
S14	18°25.907	176°43.905	2413	32	Z
S15	18°28.292	176°29.932	2540	128	Z
S17	18°31.453	176°06.278	2695	32	Z
S18	18°32.912	175°46.736	2035	128	Z
S19	18°35.998	175°24.466	2455	32	Z
S20	18°37.714	175°01.223	2074	128	Z
S21	18°40.245	174°40.803	1459	32	P
S22	18°42.029	174°22.196	1246	128	Z
Vavau	18°39.850	173°58.617	−5	25	Z
S23	18°44.232	173°39.025	2403	32	P
S24	18°44.560	173°21.725	4943	128	Z
S25	18°46.498	172°55.639	5190	32	Z
S26	18°47.968	172°22.519	5148	128	Z
S27	18°52.300	171°55.608	4698	32	Z
S28	18°54.925	171°26.017	5388	128	Z
S30	19°00.262	170°24.029	4917	128	Z

[a]Z, seismometer vertical component.
[b]P, pressure gauge.

[13] The Tonga Arc intersects the subducting Pacific plate at the Tonga Trench. There is no intervening turbidite pond, and the base of the trench contains less than 0.2 km of sediments [*Raitt et al.*, 1955]. The arc side of the trench is rocky with a 10°–12° slope, and the oceanic side has a slope of 5°–6° and is dominated by grabens up to 1 km deep created by bending-induced fracture [*Lonsdale*, 1986]. The subducting slab has been extensively studied using local and global earthquakes [e.g., *Fischer et al.*, 1991; *Koper et al.*, 1998; *Deal et al.*, 1999].

[14] The Pacific Plate is relatively flat beneath our survey line except for a large guyot at the rim of the Tonga Trench. Previous seismic measurements nearby indicate that the Pacific Plate crust is about 5 km thick and is overlain by thin sediments (0.4 km) [*Raitt et al.*, 1955]. The guyot, known as Capricorn seamount, is 4+ km tall with a 15-km-wide flat summit that tilts slightly toward the trench [*Raitt et al.*, 1955; *Wright et al.*, 2000]. This seamount is believed to have formed in the Miocene and to be part of a partially subducted hot spot chain that includes Niue Island 260 km to the east [*Brodie*, 1965]. Capricorn seamount has a limestone cap, but our study crosses a section of the flank that was probably never less than 1 km beneath the seafloor, so there are probably no significant limestones there.

3. Data Acquisition

[15] The 840-km seismic air gun line consisted of 5148 shots at a 90-s interval (160 m at 3.5 knots). The shots were generated by a 73-L array of six 10.5–13.5 L air guns at 14 MPa (2000 psi) shooting pressure. The average seismometer spacing on the line was 42 km. Each OBS contained a three-component 1-Hz geophone and a differential pressure gauge [*Cox et al.*, 1984], and the land sensor contained a broadband three-component seismometer. Some OBSs sampled at 128 Hz and some at 32 Hz, while the land station sampled at

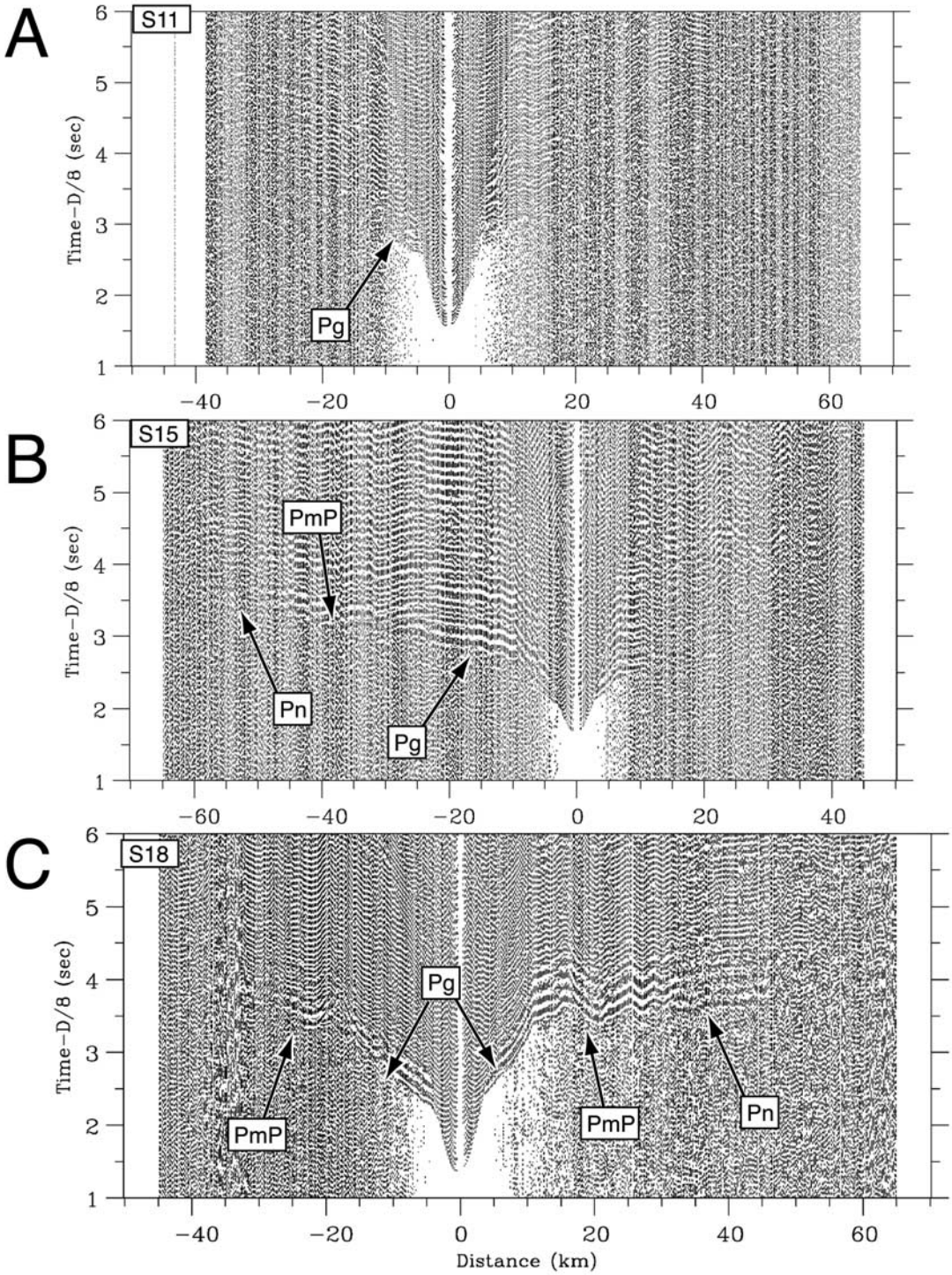

Figure 2. Wide-angle seismic record sections. *Pg* = crustal refraction, *PmP* = mantle reflection, and *Pn* = upper mantle refraction. (a) Site 11, in western Lau Basin. (b) Site 15, in Lau Basin 13 km west of the Central Lau Spreading Center. (c) Site 18, in eastern Lau Basin. (d) Site 22, on the western side of the Tonga Ridge. (e) Site 24, on the eastern side of the Tonga Ridge. (f) Site 28, on the Pacific Plate.

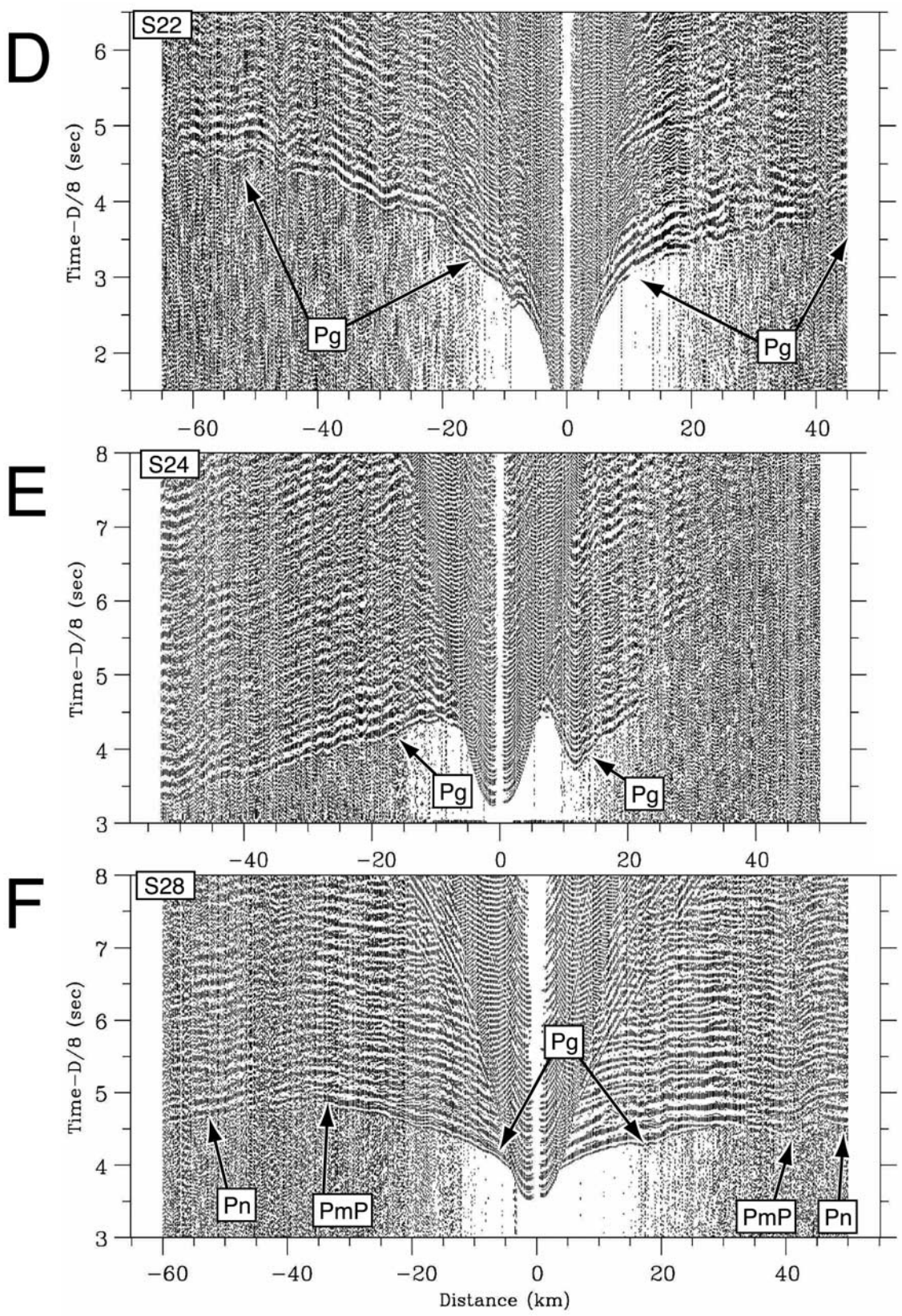

Figure 2. (continued)

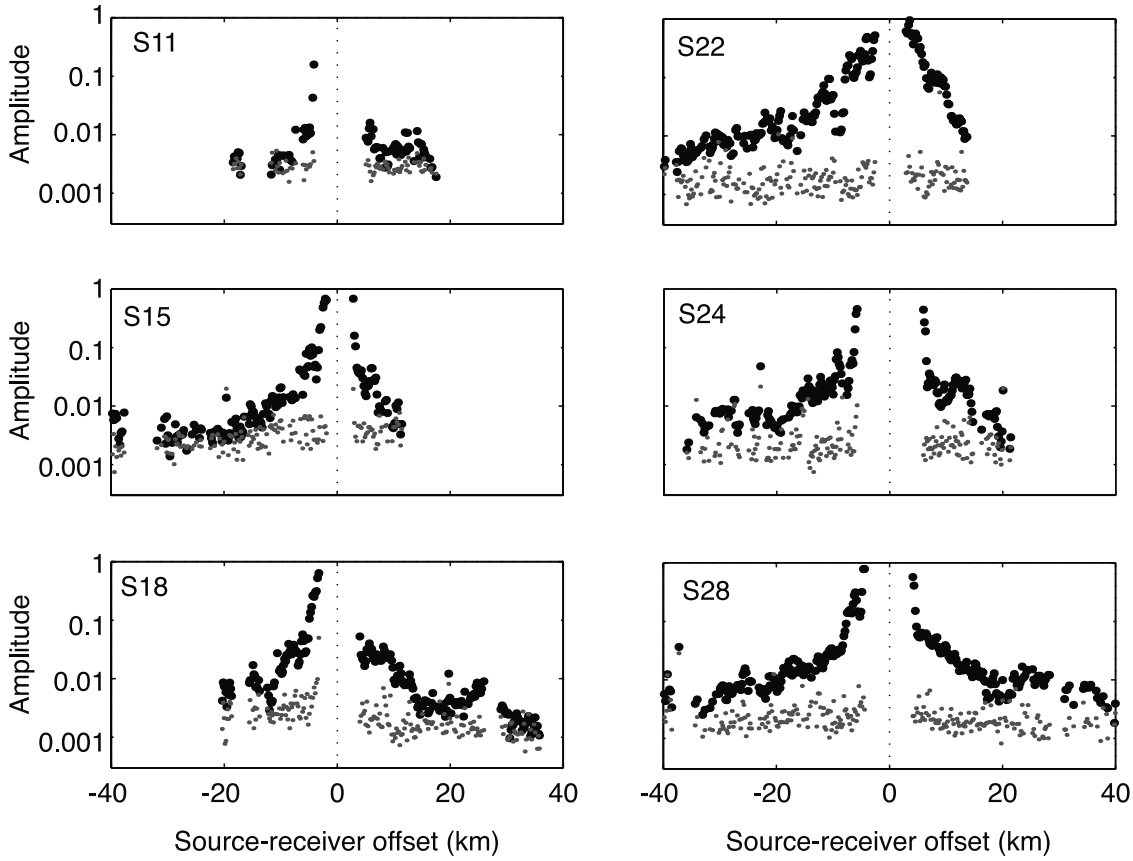

Figure 3. Amplitudes of air gun first arrivals (large solid circles) and background noise (small shaded dots) for the same sites as in Figure 2. Amplitudes are normalized with respect to the strongest water wave arrivals.

25 Hz. Table 1 shows the location, sampling rate, and best data channel of each instrument.

4. Data Processing

[16] We corrected the OBS data for clock drift and calculated instrument positions using acoustic surveys to the OBS transponders and water wave arrivals from the air gun survey. We calculated the shot locations from the shot times, P-code GPS fixes at the ship's antenna, and the towing geometry. The OBS time uncertainty is less than 10 ms, the OBS position uncertainty varies from 16 to 29 m, and the shot position uncertainty is approximately 10 m.

[17] We picked first arrivals and prominent secondary arrivals for all instruments (Figure 2) using both raw data and data filtered using a minimum phase (causal) digital filter with a passband of 5–15 Hz and a cutoff slope of 24 dB/decade [*Linville*, 1994]. We picked arrivals using the vertical seismic channel unless the pressure channel had a much better signal-to-noise ratio (Table 1). On average, shots could be picked out to 40–60 km offset. Sites on the Pacific Plate generally had the best data quality and the longest pick offsets, and sites in western Lau Basin had lower quality and the shortest offsets. To help identify arrivals in rugged areas such as the Tonga Trench, we realigned the record sections using a bathymetric correction in which the shots are relocated to the seafloor. This correction combines recursively calculated travel time-distance relations with a Fresnel zone method to calculate the mean seafloor entry point and time for the first arrivals (the geometric mean of all seafloor points whose travel time to the receiver is within one quarter phase of the fastest path) [*Sohn et al.*, 1997]. We assigned pick uncertainties as a function of the instrument sampling rate and the arrival signal-to-noise ratio (Figure 3 and Table 2) [*Zelt and Forsyth*, 1994].

5. Modeling

[18] We used a layered model inversion to fit the seismic travel times [*Zelt*, 1999]. We chose a layered model over a tomographic inversion because the ray coverage is too

Table 2. Assigned Pick Uncertainties, in Milliseconds, as a Function of Signal-to-Noise Ratio and Sampling Rate

	Instrument Sampling Rate, Hz		
Signal/Noise	128	32	25
>20	25	65	80
4–20	35	75	90
2–4	50	85	100
1.8–2	70	90	105
1.6–1.8	85	100	110
1.4–1.6	100	110	115
1.2–1.4	110	120	125
<1.2	120	130	150

sparse for a well-constrained tomographic inversion. The layered model is simpler and more stable for sparse data. The layered model also easily accounts for bathymetric effects by allowing very close node spacing at the seafloor and larger node spacing for all subseafloor elements, without any effect on the inversion stability or bias. To model ray paths in the water column, we use sound velocities measured down to 1750 m during the expedition and the Carter Table Area 54 model [*Carter*, 1980] for greater depths.

[19] We used a layer-stripping method to calculate the velocity model fitting the arrival times, starting with a single layer and adding as few and as flat constant velocity boundaries as possible to roughly fit the data. We then used a 2-D damped least squares inversion [*Zelt and Smith*, 1992] to improve the data fit by adjusting boundary depths. Unless required by the data, we did not change velocities laterally along layer boundaries. Finally, we required the inversion to reproduce crustal arrivals, sometimes at the expense of best fitting the Moho reflection arrivals. With the exception of the Moho and some sediment/rock interfaces, the model boundaries do not correspond to clear breaks in the arrival time functions, so our model only contains velocity jumps at the seafloor and at the Moho.

[20] We tried several other methods to construct velocity models, including (1) starting with a best fit model based on 1-D inversions hung from the model seafloor, (2) allowing velocities to vary laterally at each boundary node, and (3) using constant velocity layers. The method we selected gives the simplest models and the best travel time fits. In theory, a complicated model should fit data better than a simple one, but in practice inversions using more complicated models were less stable than the simple versions, probably because the 45-km OBS spacing gave relatively few ray crossings.

[21] Sediment velocities are only constrained on the Tonga Ridge, where the sediments are thick enough for us to record rays turning in the sediments. These data are best fit by a linear velocity gradient from 1.8 to 3 km/s. For lack of other constraints, we use the same boundary velocities for sediments in the rest of the model.

[22] To assure a stable inversion and to provide redundant velocity estimates, we divided the survey line into four overlapping sections, which we call West Lau, East Lau, Tonga, and Pacific (Figure 4). The West Lau section stretches from the eastern edge of the Lau Ridge to 10 km east of the CLSC, the East Lau model stretches from 25 km west of the CLSC to the Tonga Ridge, the Tonga model stretches from the eastern edge of Lau Basin to the Tonga Trench, and the Pacific model stretches from the eastern edge of the Tonga Ridge to the eastern end of the seismic line. The models overlap each other by 35–75 km (one or two OBS sites). Table 3 shows the number of rays picked and traced and the data misfit in each section.

[23] To estimate the range of possible upper mantle velocities and crustal thicknesses, we calculate the data misfit to *PmP* and *Pn* arrivals for a range of velocity and thickness values (Figure 5). The *PmP* misfit is relatively high in East Lau section, suggesting that the crust there is more complicated than our model. In Lau Basin, the best fit upper mantle velocity is 7.6–7.8 km/s. The best fit crustal thicknesses are 8.5–9.5 km beneath the WEB and the western ELSC basin, 7.5–8.5 km beneath the CLSC, and 6–6.5 km beneath eastern Lau Basin. The *Pn* arrival misfit decreases farther for upper mantle velocities slower than 7.6 km/s in eastern Lau Basin, but we reject these velocities because they require a crust so thin that many of the observed crustal arrivals are not reproduced. The best fit mantle velocities beneath eastern Lau Basin are slightly slower than those beneath western Lau Basin, but the difference is within the uncertainty bounds (Figure 5a). On the Pacific Plate, the best fit upper mantle velocity is 7.8–7.9 km/s and the crustal thickness is 5.5 km away from Capricorn seamount and up to 9 km beneath the seamount's flank.

[24] To determine the model uniqueness, we estimate node resolution (bottom rows in Figure 4) using the diagonals of the inversion resolution matrix for a depth variability of 0.1 km and a velocity variability of 0.5 km/s. A resolution value of 1.0 at a node means that if we change the depth (velocity) at that node, the resulting increase in data misfit cannot be reduced by changing the depth (velocity) at neighboring nodes. A value of 0.0 means that a change at that node can be completely compensated for by changes at other nodes. In general, a node with a resolution value >0.5 is considered to be well resolved [*Zelt*, 1999].

[25] The velocity values are generally well resolved, but the depths are not. The depth resolution is low because there are rarely more than two crossing rays at any point in the model. Moho depths are better constrained because of the simple *PmP* reflection geometry. We therefore fit the data using the smoothest possible layer boundaries. The upper crustal variations at 20 and 160 km in the West Lau section may be offset from the position indicated in our model, but their existence is well constrained because (1) we could not construct models lacking these anomalies that fit the data (either by hand or by using a Monte Carlo technique) and (2) each anomaly significantly improves the data misfit on at least two instruments.

5.1. Lau Models

[26] In the West Lau model (Figure 4a), a fairly simple velocity model fits the data well (chi-square misfit of 0.7). This model contains an eastern section with 7.5–8.5 km thick crust and a western section with 8.5–9.5 km thick crust overlain by up to 0.4 km of sediments. Most of the crustal thickening occurs in the midcrust (6–7 km/s). The boundary between these sections lies within crust created approximately 1.8 Ma at the ELSC, approximately 50 km west of the present-day CLSC [*Zellmer and Taylor*, 2001]. The model contains three localized upper crustal velocity anomalies, each of which is required to fit clear travel time breaks on more than one instrument. If we remove these anomalies, the chi-square error increases to 1.27.

[27] A chi-square error less than 1 suggests that the model overfits the data; that is, either the model is too complicated or the estimated uncertainties are too large. Since our model is less complicated than that suggested by drilling and dredging [*Hawkins*, 1995], we believe that we have overestimated the pick uncertainties. We could reduce these uncertainties to force a higher error estimate, but we opt to use the same uncertainty formula (Table 2) for all

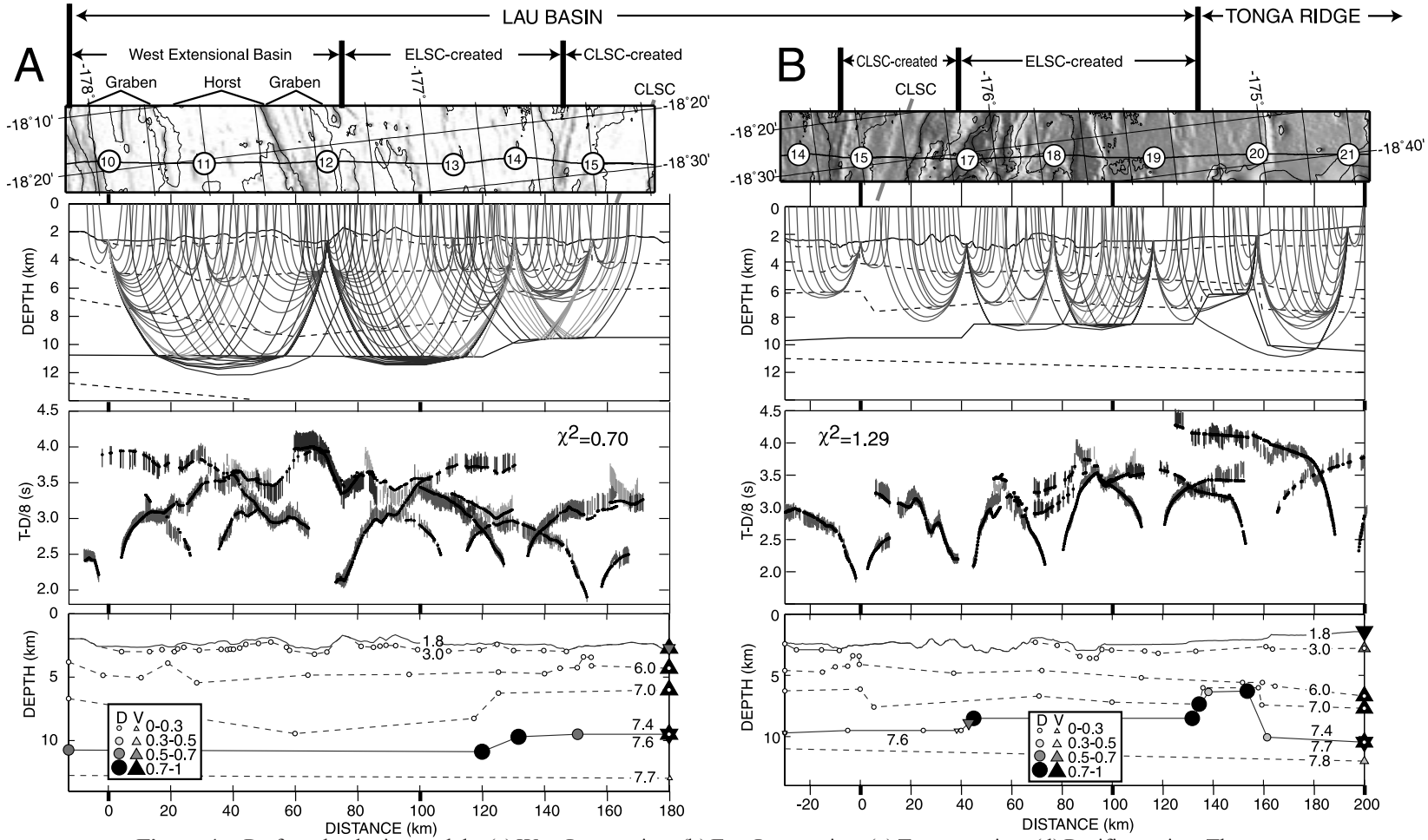

Figure 4. Preferred velocity models: (a) West Lau section, (b) East Lau section, (c) Tonga section, (d) Pacific section. The top plot shows the bathymetry [*Zellmer and Taylor*, 2001], OBS locations (circles), and the air gun line (solid line). The second plot shows ray paths (every fifth ray) and the velocity model. Dashed lines indicate layer boundaries with continuous velocities; solid lines indicate boundaries with velocity discontinuities. Colored lines trace the modeled ray paths (red = *Pg* (crust), green = *PmP* (Moho reflections), blue = *Pn* (crust-mantle)). The third plot shows the data fit, with measured travel times and their uncertainty shown in color and the modeled arrival times shown in black. The bottom plot shows uncertainty estimates calculated from the resolution matrix (larger symbols indicate better resolution): circles = depth nodes, upward pointing triangles = velocity at the bottom of the overlying layer, downward pointing triangles = velocity at the top of the underlying layer [*Zelt*, 1999]. Where there is only one type of triangle, velocity is continuous across the boundary. Constant velocity boundaries only have triangles at the right edge. If two boundaries "pinch out" together (usually at the seafloor), we moved the triangle for the upper boundary to the point of easternmost separation of the layers. In the legend, D = depth and V = velocity. See color version of this figure at back of this issue.

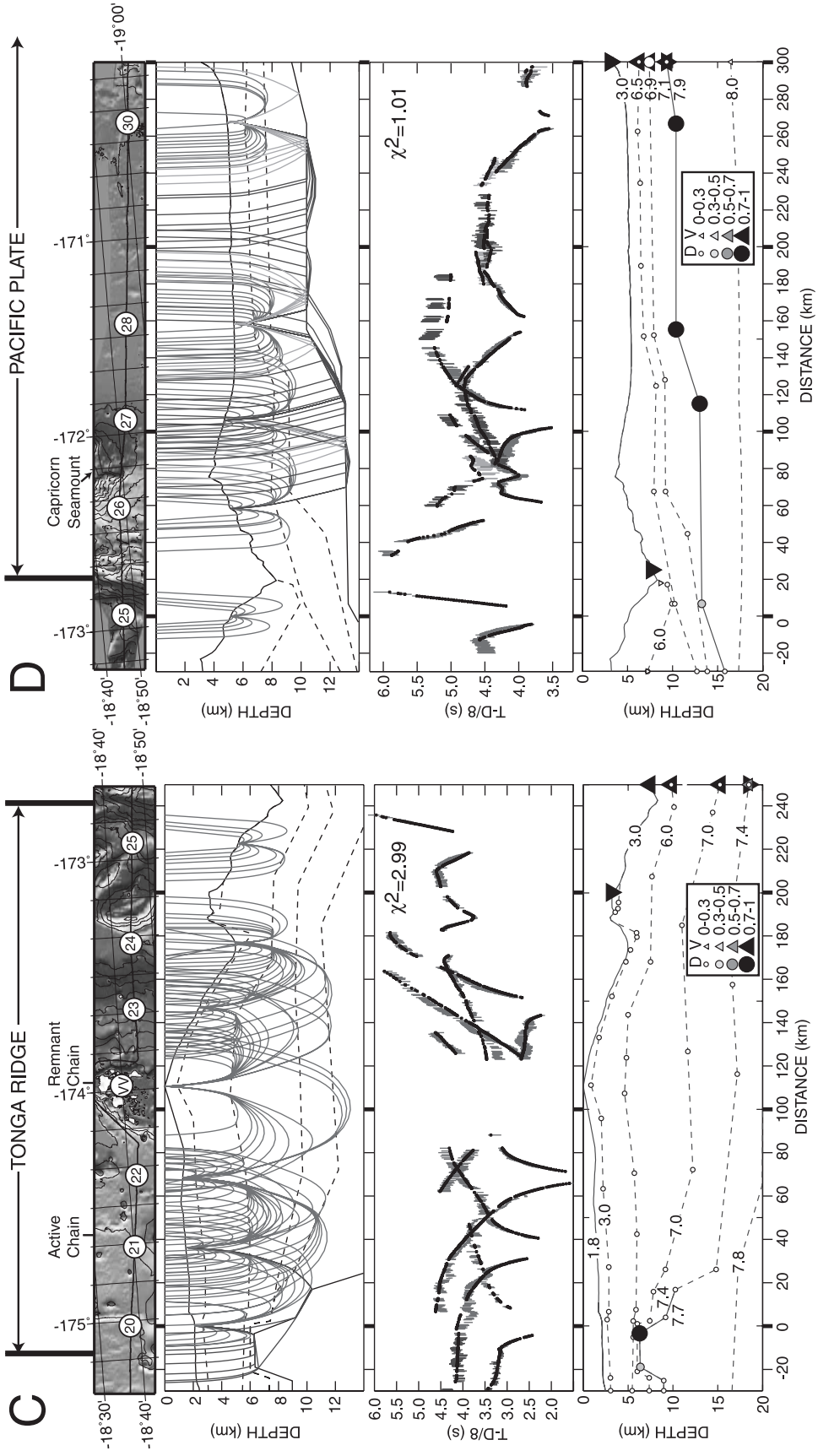

Figure 4. (continued) See color version of this figure at back of this issue.

Table 3. Ray and Pick Statistics for the Final Velocity Models

	West Lau			East Lau			Tonga			Pacific		
	Pg	*PmP*	*Pn*	*Pg*	*PmP*	*Pn*	*Pg*	*PmP*	*Pn*	*Pg*	*PmP*	*Pn*
Arrivals picked	946	168	310	1018	112	231	1269	0	124	802	146	297
Rays traced	903	155	305	885	57	196	1217	0	99	733	146	261
RMS residual, ms	63	116	83	77	110	59	96	NA	47	59	68	81
χ^2 error	0.63	1.10	0.70	1.22	4.93	0.59	3.20	NA	0.50	1.06	1.10	0.80

four model sections. This formula is based on handpicked uncertainty estimates for the ensemble of the data.

[28] The data do not fit a previously proposed seismic velocity model for the WEB, which was based on seismic reflection and borehole data [*Shipboard Scientific Party*, 1992b, 1992a]. In that model, the basalt velocities are greater than 4.2 km/s, the grabens are filled with 0.12–0.16 km of very slow sediments (1.5–1.6 km/s), and the horsts are sediment-free. The short-range arrival times for this model approximately fit the travel times to site 12, but our data require (1) thicker (0.2–0.3 km) sediments in the graben containing site 10, and (2) crustal velocities slower than 4.2 km/s beneath the site 11 horst.

[29] In the East Lau model (Figure 4b), the crust thins to the east and is very thin (4–4.5 km) at the boundary between Lau Basin and the Tonga Ridge (Figure 4b, x = 145 km). This very thin crust, required to fit a break in the travel time curve at site 20 (Figure 6), was previously revealed by a 1-D seismic survey approximately 90 km to the south [*Pontoise and Latham*, 1982, Figures 1 and 7A, site P17]. A sediment layer begins approximately 65 km west of the Tonga Ridge boundary (Figure 4b) and thickens to the east.

[30] *PmP* errors are very large in the East Lau section (Table 3 and Figure 4b), because we could not create a model fitting the *Pg* arrivals that also had *PmP* arrivals as early as those observed west of site 18. To better fit the *PmP*

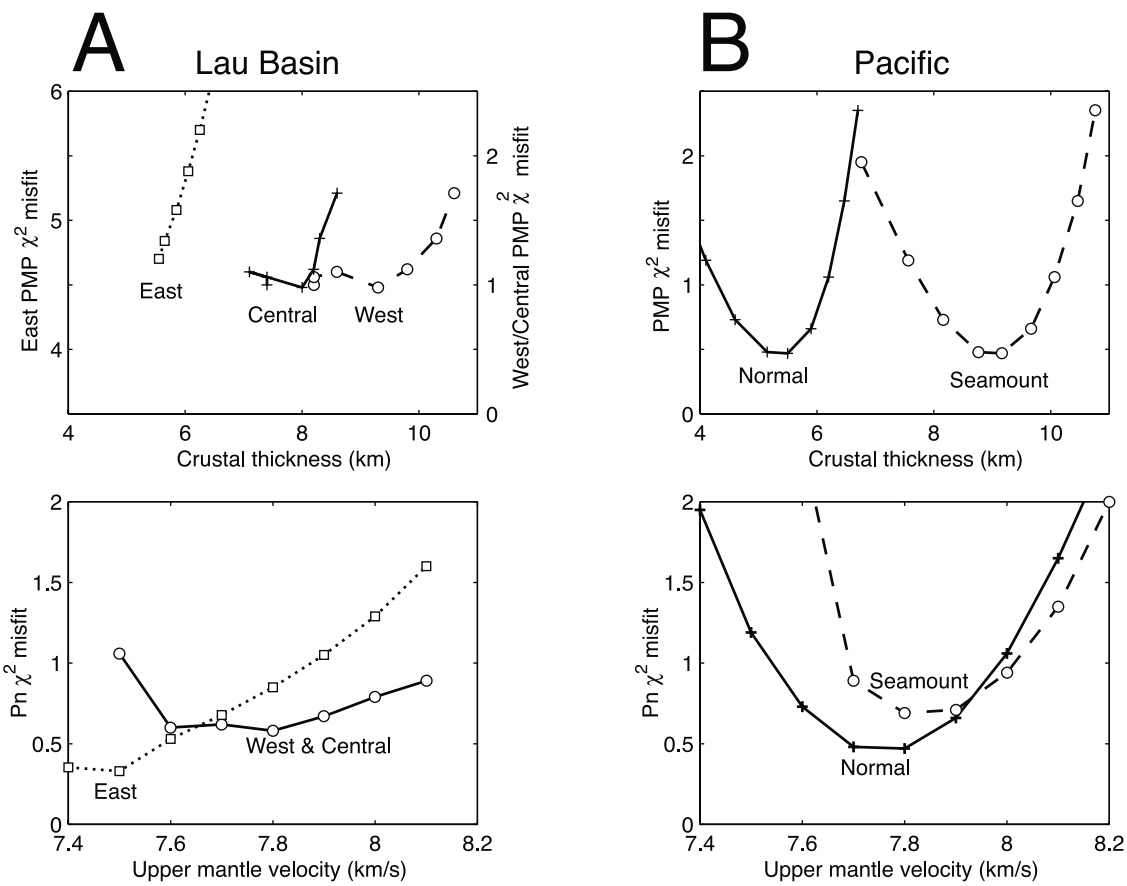

Figure 5. Effect of changes in model crustal thickness (top row) and upper mantle velocity (bottom row) on data misfit. (a) Lau Basin. "West" and "Central" data are from 20–120 km and 130–160 km, respectively, in the West Lau section (Figure 4a). "East" data are from 50–120 km in the East Lau section (Figure 4b). Crustal thicknesses are calculated relative to the average Lau Basin seafloor depth of 2.2 km. (b) Pacific Plate. "Seamount" and "normal" data are from 60–100 km and 160–260 km, respectively, in the Pacific section (Figure 4d). Seamount crustal thickness is calculated relative to the shallowest seafloor depth of 4 km.

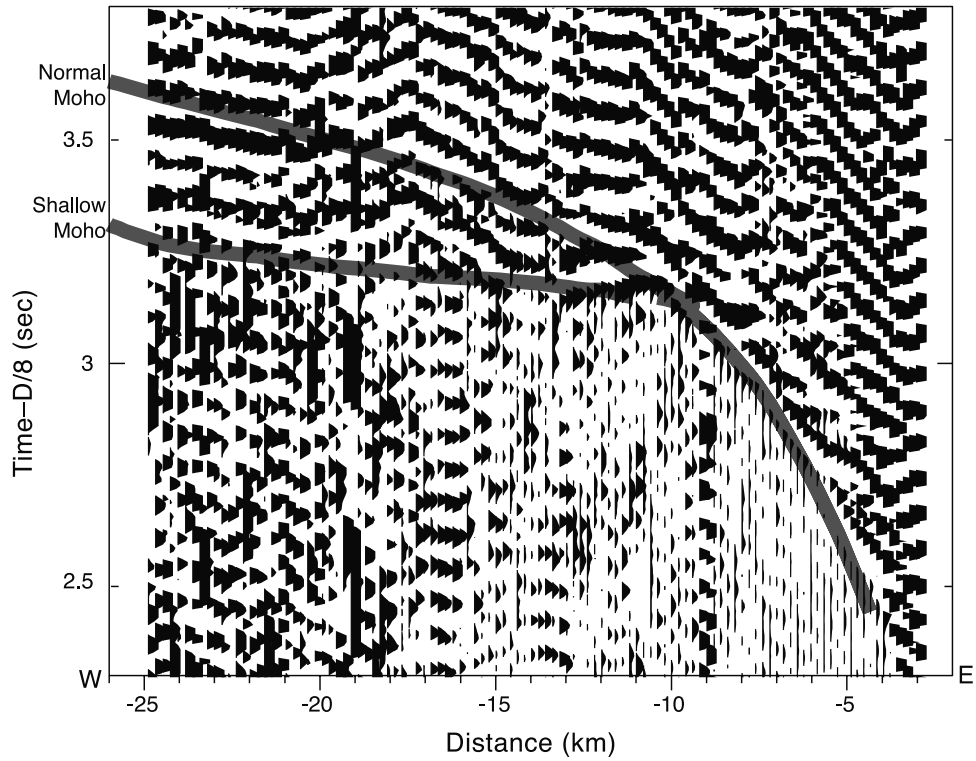

Figure 6. Site S20 record section showing the effect of the shallow Moho at the eastern edge of Lau Basin. The shaded lines show arrival times for models with and without the shallow Moho.

arrivals, we would have to impose a thinner crust or higher lower crust velocities, neither of which is consistent with the crustal arrivals.

5.2. Tonga Model

[31] The Tonga model (Figure 4c) reveals that the crust thickens rapidly beneath Tonga Ridge, that the sediment layer thickness varies significantly, and that the intermediate-velocity (6–7 km/s) layer is very thick. The sediment layer is up to 1 km thick on the west side of this chain and is generally thinner and more variable to the east. Rays turning in the sediments beneath site 21 are best fit by a linear gradient from 1.8 km/s at the surface to 3.0 km/s at its base. The intermediate velocity layer is thickest (7.5 km) beneath the remnant volcanic chain. Our model velocities generally match those obtained from previous 1-D seismic studies (Figure 7).

[32] The Tonga model has a chi-square misfit of 2.99, the highest of the four models. Most of the misfit comes from short-wavelength arrival time variations. A more complicated model is needed to fit these variations, but our ray coverage is too sparse to uniquely constrain the necessary model variations. The sediment thickness probably varies much more than in our model [*Pontoise and Latham*, 1982], but there might be significant lower crustal variations as well. We believe that our model is a smoothed version of the actual structure, because it fits the overall trends quite well with a minimum of structure.

5.3. Pacific Model

[33] The Pacific model (Figure 4d) reveals typical oceanic crust to the east (5–6 km thick) and crust up to 9 km thick beneath Capricorn seamount. The Pacific crust velocity profile consists of a 1- to 1.5-km-thick upper crust (3–6.5 km/s), 1- to 1.5-km-thick midcrust (6.5–6.9 km/s), and 2.5- to 3-km-thick lower crust (6.9–7.1 km/s). Beneath Capricorn seamount, the upper and lower crust thicken to 4 km each, while the midcrustal layer does not thicken but dives 1–1.5 km deeper with respect to the sea surface.

[34] Previous seismic studies indicate that the Pacific crust in the area is covered by a thin sediment veneer (0.4 km) [*Raitt et al.*, 1955]. No sediments are required in the 2-D model, which ignores subtle breaks in the travel time curves. Since the seafloor is relatively flat between sites 28 and 30, we also built 1-D models based on ray entry points between these sites. We relocated the shots to the seafloor using a Fresnel zone method [*Sohn et al.*, 1997], then recalculated travel times and distances from these seafloor shot points. The line fitting the first arrivals does not pass through the origin, indicating that no rays turn in the top layer, so we assume that this top layer consists of sediments with a velocity of 2.5 km/s [*Raitt et al.*, 1955]. The site 28 data are best fit by a 0.3-km-thick sediment layer, whereas the site 30 data are best fit by 0.15 km of sediments. Both sites require four layers beneath the sediments, with velocities similar to the typical oceanic crustal sequence of basalts (5–6 km/s), diabase (6.3–6.8 km/s), gabbros (6.8–7.2 km/s), and upper mantle peridotites (7.8–8.2 km/s) [*Spudich and Orcutt*, 1980]. In both cases, the upper/middle crust (<6.8 km/s) is 2–2.5 km thick and the lower crust (>6.8 km/s) is 3 km thick, in agreement with the 2-D model.

5.4. Overall Model

[35] We combine the four model sections into an overall crustal model (Figure 8). Figure 9 and Table 4 show typical

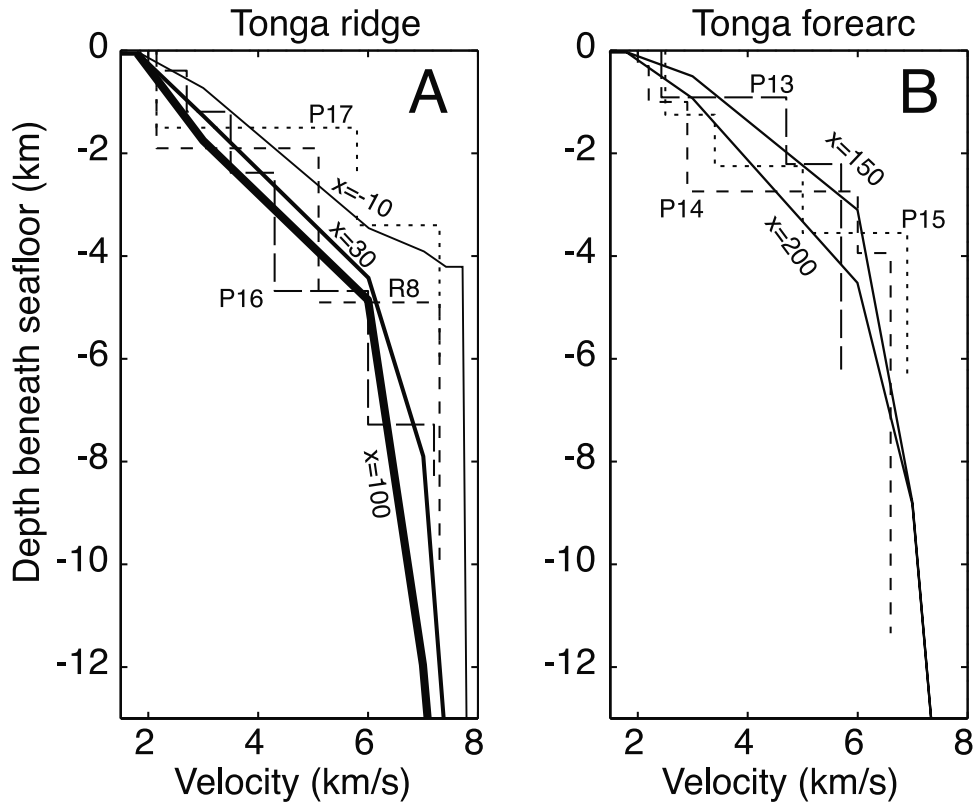

Figure 7. Tonga Ridge velocity profiles compared to profiles from previous 1-D seismic studies. Left plot shows models from the western half of the chain; right plot shows models from the eastern half. "P" models are from *Pontoise and Latham* [1982], model R8 is from *Raitt et al.* [1955] (see Figure 1 for their location). Solid lines are from our 2-D model. The distances shown indicate the position of our profiles within the Tonga model (Figure 4c).

velocity profiles for each major model unit. The most important model features are as follows:

[36] 1. The Pacific crust is 5.5 km thick, with a relatively thin midcrust (1–1.5 km) and less than 0.4 km of sediments.

[37] 2. The Pacific crust thickens to 9 km beneath the flank of Capricorn seamount. The thickening is restricted to the upper and lower crust, while the midcrust deflects 1.5 km deeper.

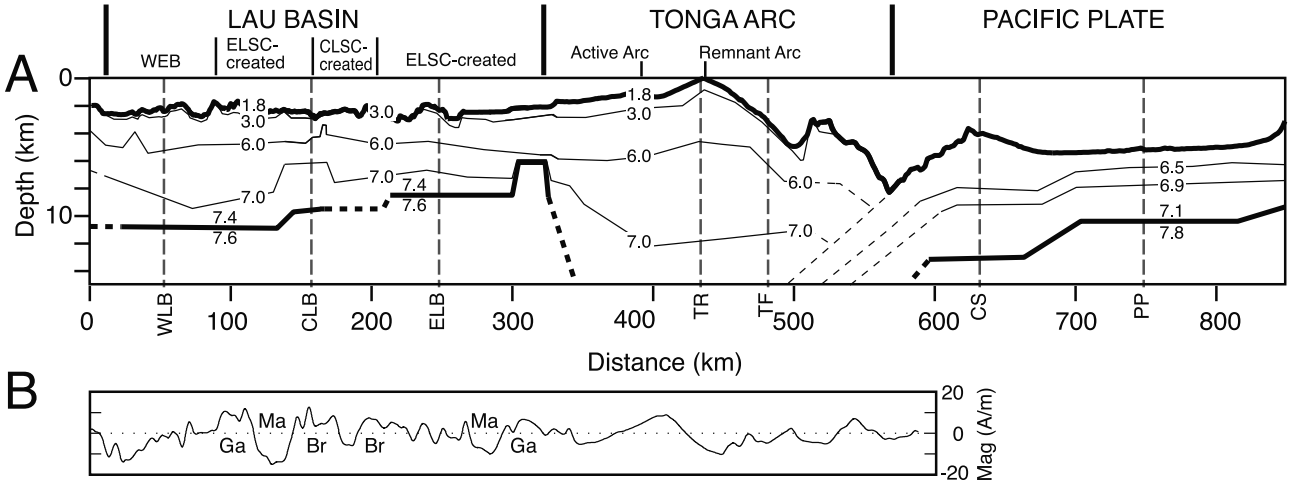

Figure 8. Overall velocity model. (a) Two-dimensional cross section. Bold lines show the seafloor and the Moho, and thin lines show second-order velocity boundaries. Lines are solid where they are sampled by rays and dashed where they are not. The shaded dashed vertical lines mark the position of the velocity profiles shown in Figure 9 and Table 4. (b) Inferred seafloor magnetization (A/m) along the survey line, with Brunhes (BR), Matuyama (Ma), and Gauss (Ga) periods identified [from *Zellmer and Taylor*, 2001].

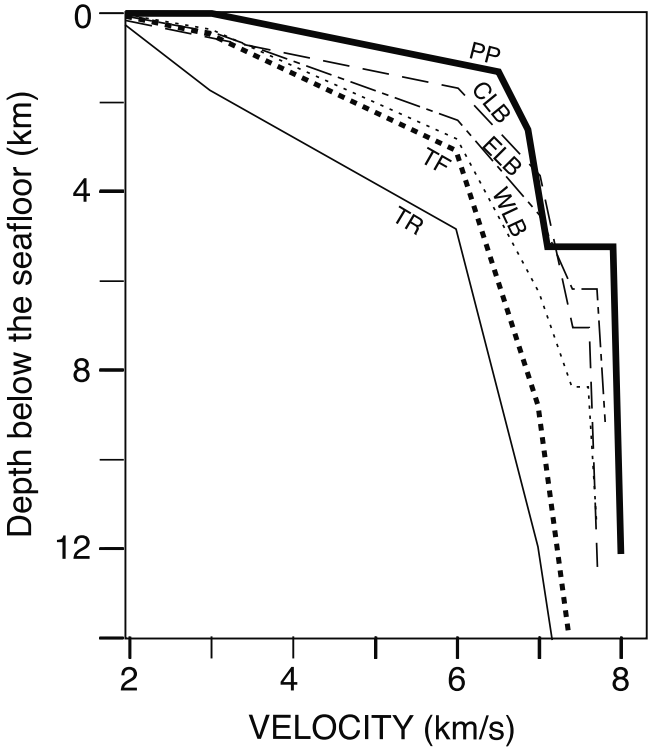

Figure 9. One-dimensional velocity profiles from the overall model (positions indicated in Figure 8). Abbreviations are TR, Tonga Ridge; TF, Tonga Forearc; WLB, western Lau Basin; ELB, eastern Lau Basin; CLB, central Lau Basin; PP, Pacific Plate.

[38] 3. The Tonga Ridge contains a thick intermediate-velocity layer (6–7 km/s, up to 7.5 km thick) beneath the Tonga Ridge. This layer is thickest beneath the remnant volcanic arc.

[39] 4. At the boundary between Lau Basin and the Tonga Ridge, the crust is exceptionally thin (~4 km).

[40] 5. In Lau Basin the crustal thickness increases from 6 km in the east to 9 km in the west. All of the Lau Basin crust has a thicker midcrustal section than is seen in the Pacific Plate. Crustal thickening between the eastern and central sections is concentrated in the lower crust, while crustal thickening between the central and western sections occurs in the midcrust.

6. Discussion

[41] We present an interpretive model of the Tonga-Lau crustal structure in Figure 10, based on the model velocities and the lithologies expected in each tectonic setting. The principal features of this model are the andesitic rocks beneath the Tonga Ridge, the existence of a mantle melt source west of the Lau Basin spreading center, the variations in crustal thickness in Lau Basin, and the very thin crust at the boundary between Lau Basin and the Tonga Ridge. We will first discuss the "oceanic" crust of the Pacific Plate and Lau Basin and then the Tonga Ridge.

6.1. Pacific Plate and Capricorn Seamount

[42] The seismic velocities in the Pacific plate crust away from Capricorn seamount are similar to the "generic" Pacific crust velocities indicated by numerous other seismic studies and correlate well to the inferred lithology of the present EPR [*Spudich and Orcutt*, 1980; *Harding et al.*, 1993]. The thickness and seismic velocity of the upper section match those of rise axis extrusive basalts (3–6.5 km/s and 1–1.5 km thick), the parameters of the middle section match those of intrusive diabase dikes (6.5–6.9 km/s and 1.5 km thick), and the lower section velocities match those of plutonic gabbros (6.9–7.1 km/s). These associations are approximate since one can trade off model layer velocities and depths, but they correspond well to standard models. The lower crust, however, is relatively thin (2.5 km versus 3–5 km for the EPR).

[43] Where the seismic line crosses the flank of Capricorn seamount, the upper and lower crusts thicken to nearly 4 km each. The midcrustal layer does not thicken, but it deepens by 1.5 km with respect to the sea surface. The constant thickness and the deflection of this layer suggest that the oceanic crust here is relatively unaltered and has been loaded from above by surface lava flows. The most likely explanation for the thickening of the lower crust is magmatic underplating during the volcanic phase. Alternatively, the lower crust may have thickened through serpentinization of mantle peridotites by deep hydrothermal circulation, but there is no compelling reason why hydrothermal fluids

Table 4. Velocity Profiles From Representative Sections of the Model (Same as in Figure 9)

West Lau Basin (WL)		Central Lau Basin (CL)		East Lau Basin (EL)	
Depth, km	Velocity, km/s	Depth, m	Velocity, km/s	Depth, m	Velocity, km/s
0.0	1.8	0.0	1.8	0.0	1.8
0.4	3.0	0.5	3.0	0.4	3.0
2.9	6.0	1.7	6.0	2.4	6.0
6.2	7.0	3.7	7.0	4.5	7.0
8.4	7.4/7.6	7.1	7.4/7.6	6.1	7.4/7.6

Tonga Ridge (TR)		Tonga Forearc (TF)		Capricorn Seamount (CS)		Pacific Plate (PP)	
Depth, m	Velocity, km/s	Depth, m	Velocity, km/s	Depth, m	Velocity, km/s	Depth, m	Velocity, km/s
0.0	1.8	0.0	1.8	0.0	3.0	0.0	3.0
0.8	3.0	0.4	3.0	4.0	6.5	1.3	6.5
4.9	6.0	3.1	6.0	5.2	6.9	2.6	6.9
12.0	7.0	8.8	7.0	9.1	7.1/7.8	5.2	7.1/7.8

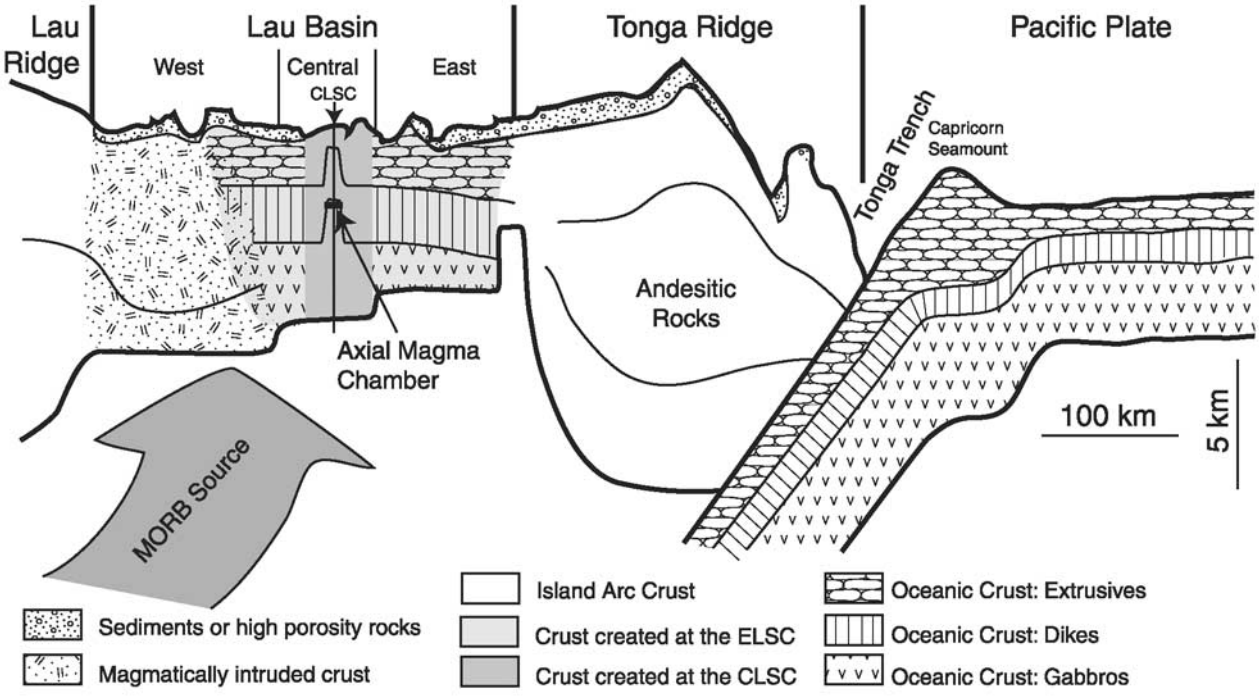

Figure 10. Interpretive model. The Pacific Plate and central-east Lau Basin are interpreted as oceanic crust created at magma-rich spreading centers. Capricorn seamount creates a thicker extrusive and plutonic crust. In Lau Basin, variations in the thickness of crustal layers may reflect changes in the amount of melt available and the depth of the axial melt lens at the spreading ridge. West Lau Basin contains a mixture of crust created at an oceanic spreading center and extended arc crust, both overprinted by recent volcanism from a mantle source centered west of the current oceanic spreading center. The Tonga Ridge contains a thick layer of andesitic rocks similar to that observed beneath the Izu-Ogasawara Ridge [*Suyehiro et al.*, 1996].

would circulate this deep in the relatively low stress intraplate environment where the seamount formed.

6.2. Lau Basin

[44] The Lau Basin crust thickens from east to west in two steps. We use these steps to divide the basin into east, central, and west sections (5.5–6.5, 7.5–8.5, and 9 km thick, respectively). The boundary between the east and central sections lies at the boundary between crust created at the ELSC and the CLSC, suggesting these two spreading ridges have or had different internal structures. The boundary between the central and west sections, on the other hand, lies in the middle of crust created at the ELSC. The west section therefore contains crust created both by oceanic spreading and by island arc extension.

[45] The east section crust is about as thick as the Pacific Plate crust, but the upper and middle crust are thicker (2–2.5 km each) and the lower crust is thinner (1.5–2km). The travel time data also require different boundary velocities than those seen in the Pacific crust, which may indicate a different source chemistry or emplacement mechanism. If the boundary between the middle and lower crust corresponds to the position of the melt lens at the spreading ridge, the ridge that created the east section crust had a deeper melt lens than the ridge that created the Pacific crust. The upper and middle crust total 4–5 km thick, suggesting that the source melt lens was between 2.5 and 4.5 km deep, depending on how much upper crust was emplaced off-axis. This is consistent with present-day estimates of the melt lens depth near the south end of the ELSC (2.9 ± 0.3 km [*Turner et al.*, 1999]). However, the lower crust is much thinner beneath our East Lau section (1.5–2 km versus 5–6 km).

[46] The central section contains mostly crust created at the CSLC. The average crustal thickness is 7.5–8.5 km. Most of the thickening between the east and central sections takes place in the lower crust: The upper crust and most of the middle crust are actually thinner in the central section, suggesting a shallower source melt lens. A CLSC melt lens has been imaged 1.1–1.7 km beneath the seafloor at these latitudes [*Harding et al.*, 2000], even shallower than our midcrustal thickness. This difference might be explained by a recent change in the melt structure of the CLSC, corresponding to a recent change in the spreading rate. The present-day spreading rate (from GPS measurements [*Bevis et al.*, 1995]) is much faster than the long-term rate (from seafloor magnetization [*Taylor et al.*, 1996]), suggesting that the spreading rate may have recently accelerated. In addition, the upper crust is very thin beneath the OBS closest to the CLSC axis (site 15, Figure 4a). This thin upper crust could reflect a change in the melt structure near the rise axis, but our data do

not constrain whether this thin layer extends to the CSLC or if the middle crust is also thinner beneath the rise axis, as would be expected for the present melt lens depth.

[47] The Lau Basin crust is thickest (9 km) in the west section, which contains both the West Extensional Basin (WEB) and crust created more than 1.5 Ma on the west side of the ELSC. Most of this crust has intermediate velocities (6–7 km/s). Within this section, there is no significant change in crustal thickness or velocity structure between the crust created in the WEB and that formed at the ELSC, suggesting that the crust was modified postemplacement. The most likely source of this modification is the mantle source centered west of the Lau Basin spreading axis. This source was active in the past, as indicated by Pacific-type MORB sampled within the WEB grabens [*Hawkins*, 1995], and it may still be active, as indicated by a low-velocity anomaly imaged in the upper mantle west of the CLSC [*Zhao et al.*, 1997]. We suggest that this melt supply modified both the WEB and the ELSC crust within the west section and that it may continue to modify this crust today.

[48] Isostasy predicts that the increase in thickness of Lau Basin crust toward the west should result in shallower seafloor depths to the west, but no such trend is observed. The effect of this thickening is relatively small because most of the thickening occurs in the denser middle and lower crust and the eastern Lau Basin crust has the thickest low-velocity (and probably low-density) layer. However, assuming average midcrustal, lower-crustal, and upper mantle densities of 2.75, 3.35 and 3.7 g/cm^2, respectively [*Christensen and Smewing*, 1981], the seafloor should deepen by approximately 0.8 km from west to east. If the sediment layer overlying eastern Lau Basin has very low density (1.8 g/cm^2), this difference reduces to 0.6 km, but even this small a change is not observed. Dynamic compensation beneath the eastern basin seems unlikely since the only imaged mantle low-velocity anomaly is beneath the western basin [*Zhao et al.*, 1997]. For lack of a better explanation, we speculate that crustal and/or mantle densities decrease toward the east because of compositional differences in the mantle from west to east. Since the eastern Lau Basin crust shows no evidence of significant change since emplacement, we speculate that the material emplaced in the western Lau Basin crust may be relatively dense. To date, there have been no gravitational studies to test this hypothesis.

[49] In summary, the melt supply to the Lau Basin spreading ridges has changed significantly over time and a large portion of the crust west of the spreading ridge appears to have been modified by melt emplacement after formation. The westward offset of the melt supply may be the result of the massive cold barrier formed by the subducting slab to the east and may therefore be a common feature of back arc spreading centers. If this is the case, crust created in back arc basins should be systematically different than that formed by "normal" oceanic spreading.

6.3. The Tonga Ridge-Lau Basin Boundary

[50] Why is the crust thinned at the boundary between Lau Basin and the Tonga Ridge? It may be related to the start of spreading, since this crust was probably created near the time when the propagating tip of the ELSC arrived from the north. Perhaps there was an impulse of previously trapped mantle melt as the ELSC propagated south. Or perhaps crust created by an isolated magmatic impulse was subsequently thinned by extension. A more detailed study of this feature would help to reveal its source and could provide information about how seafloor spreading starts. It would be interesting to determine if this feature is unique to Tonga-Lau or if it exists at other arc-back arc boundaries.

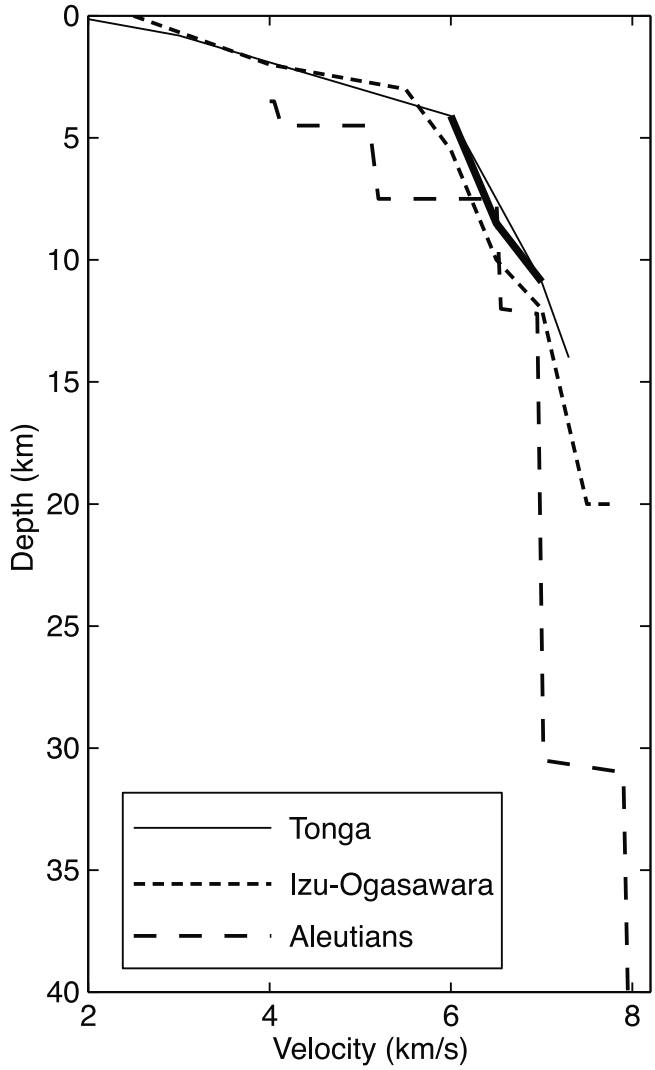

Figure 11. Comparison of the velocity profile beneath the remnant island arc of the Tonga Ridge with profiles from the Aleutian [*Holbrook et al.*, 1999] and Izu-Ogasawara arcs [*Suyehiro et al.*, 1996]. The bold solid line shows an alternative version of the Tonga Ridge midcrust with a thicker 6–6.5 km/s layer whose misfit is within 1% of the best value.

6.4. Tonga Ridge

[51] The velocity profile beneath the Tonga Ridge strongly resembles that beneath the Izu-Ogasawara arc [*Suyehiro et al.*, 1996] (Figure 11). Both volcanic arcs contain a thick layer of relatively low velocities starting 4–5 km beneath the seafloor. *Suyehiro et al.* [1996] suggest that this layer consists of tonalites within the Izu-Ogasawara arc because tonalites outcrops were found on that arc and because the

velocities correspond much better to andesitic than to basaltic rocks at those depths [*Christensen and Mooney*, 1995]. The Tonga velocities may be even closer to those at Izu-Ogasawara than suggested by our model. The data fit hardly changes (from chi-square = 2.99–3.02) if we copy the Izu-Ogasawara model structure by emplacing a 6–6.5 km/s layer that is up to 5 km thick (bold solid line, Figure 11).

[52] The existence of andesitic rocks beneath island arcs is crucial to a hypothesis that continental crust is formed through accretion of successive island arcs. The existence of low-velocity layers beneath both the Tonga Ridge and the Izu-Ogasawara arc supports this hypothesis, but other island arcs, such as the Aleutian arc (Figure 11)], show no 6–6.5 km/s layer [*Holbrook et al.*, 1999]. Large-scale crustal velocity studies at other arcs should help to determine the factors that control the generation of andesitic rocks.

[53] Our data do not constrain the thickness of the Tonga Ridge, but previous studies indicate that it is between 20 and 25 km thick [*Raitt et al.*, 1955; *Mitronovas and Isacks*, 1971]. For comparison, the Izu-Ogasawara arc crust, which has a similar velocity structure, is approximately 22 km thick [*Suyehiro et al.*, 1996].

7. Conclusions

[54] We conducted a seismic refraction (air gun) survey to 19 OBSs and one land seismometer across the Tonga-Lau subduction/back arc system. Beneath our survey line, the Pacific Plate crust approaching the Tonga Trench is 5.5 km thick and the crust thickens to 9 km beneath the southern edge of Capricorn seamount, with 1.5–2 km of thickening in both the upper and lower crust. The midcrust does not thicken but deepens by 1.5 km beneath the edifice. The excess upper crust is probably lava flows from the seamount, while the excess lower crust is probably underplated gabbros but could also be serpentinized mantle peridotites.

[55] The Tonga Ridge contains a thick layer of rock whose low velocity matches that of andesitic rocks in continental crust. The velocity structure of the Tonga Ridge is strikingly similar to that of the Izu-Ogasawara arc, which has been interpreted to contain andesitic rocks.

[56] There is a section of extremely thin crust (4–4.5 km) between Lau Basin and the Tonga Ridge. This thin crust formed when seafloor spreading started with the arrival of the southward propagating tip of the ELSC.

[57] The Lau Basin crust thickens from 5.5–6.5 km in the east to 8.5–9.5 km in the west. The basin is divided into east, central, and west sections by steps in the crustal thickness. In the east section, the crust resembles that seen in the Pacific Plate east of the Tonga Trench, except that the midcrustal layer is thicker and the lower crust is thinner. We interpret this as oceanic crust created more than 1.5 Ma at the ELSC with a melt lens 2.5–4.5 km deep. The crust is 1 km thicker in the central section, due mostly to a thicker lower crust. Most or all of this crust formed within the past 1.5 Ma at the CLSC, and we interpret the difference between these sections as reflecting the difference between the rise axis structure at the ELSC more than 1.8 Ma and that at the CLSC within the past 1Ma. The upper crust thins by 1 km within 5 km of the CLSC, perhaps reflecting a recent (~0.1 Ma) change in spreading center structure. Lau Basin crust thickens to approximately 9 km in the west section. The primary difference between the west section and the rest of Lau Basin is in the midcrust, which is 2 km thick beneath the east and central sections and up to 5 km thick beneath the west section. The west section contains both crust formed at the ELSC more than 1.5 Ma and crust formed through extension of the original Lau Ridge. We suggest that these originally different crusts were modified postemplacement by infilling of melt from a robust mantle melt supply west of the CLSC.

[58] **Acknowledgments.** We thank the captain and crew of the R/V *Melville* for their competent work and assistance during the WESTWARD 6 cruise. We thank Perry Crampton for preparing, operating, and nursing the air guns. Chris Bradley, Sharon Escher, Tevita Fatai, Peter Hill, Javier Porras, Allan Sauter, Robert Sohn, Kimberley Williams, and Bob Wilson helped with instrument preparation and deployments as well as shipboard data collection. We thank James Hawkins for discussions and information and Martin Sinha, Yosio Nakamura, and an anonymous reviewer for thoughtful and insightful reviews of the original manuscript. This research was funded by NSF grants OCE9314399 and OCE0002878.

References

Barth, G. A., and J. C. Mutter, Variability in oceanic crustal thickness and structure: Multichannel seismic reflection results from the northern East Pacific Rise, *J. Geophys. Res.*, *101*(8), 17,951–17,975, 1996.

Bevis, M., et al., Geodetic observations of very rapid convergence and back-arc extension at the Tonga arc, *Nature*, *374*, 249–251, 1995.

Brodie, J. W., Capricorn seamount, south-west Pacific Ocean, *Trans. R. Soc. N. Z. Geol.*, *3*(10), 151–158, 1965.

Carter, D. J. T., *Echo-Sounding Correction Tables*, Hydrograph. Dep., Minist. of Def., UK, 1980.

Christensen, N. I., and W. D. Mooney, Seismic velocity structure and composition of the continental crust: A global view, *J. Geophys. Res.*, *100*(7), 9761–9788, 1995.

Christensen, N. I., and J. D. Smewing, Geology and seismic structure of the northern section of the Oman ophiolite, *J. Geophys. Res.*, *86*(4), 2545–2555, 1981.

Collier, J. S., and M. C. Sinha, Seismic mapping of a magma chamber beneath the Valu Fa Ridge, Lau Basin, *J. Geophys. Res.*, *97*(10), 14,031–14,053, 1992.

Cox, C. S., T. Deaton, and S. C. Webb, A deep sea differential pressure gauge, *J. Atmos. Oceanic Technol.*, *1*, 237–246, 1984.

Deal, M. M., G. Nolet, and R. D. van der Hilst, Slab temperature and thickness from seismic tomography: 1. Method and application to Tonga, *J. Geophys. Res.*, *104*(12), 28,789–28,802, 1999.

Fischer, K. M., K. C. Creager, and T. H. Jordan, Mapping the Tonga slab, *J. Geophys. Res.*, *96*(9), 14,403–14,427, 1991.

Harding, A. J., G. M. Kent, and J. A. Orcutt, A multichannel seismic investigation of upper crustal structure at 9 degrees N on the East Pacific Rise: Implications for crustal accretion, *J. Geophys. Res.*, *98*(8), 13,925–13,944, 1993.

Harding, A. J., G. M. Kent, and J. A. Collins, Initial results from a multichannel seismic survey of the Lau back-arc basin, *Eos Trans. AGU*, *81*(48), Fall Meet. Suppl., Abstract T61C-16, 2000.

Hawkins, J. W., The geology of the Lau Basin, in *Backarc Basins: Tectonics and Magmatism*, edited by B. Taylor, pp. 63–138, Plenum, New York, 1995.

Holbrook, W. S., et al., Structure and composition of the Aleutian island arc and implications for continental crustal growth, *Geology*, *27*(1), 31–34, 1999.

Karig, D. E., Ridges and basins of the Tonga-Kermadec island arc system, *J. Geophys. Res.*, *75*(2), 239–254, 1970.

Kent, G. M., A. J. Harding, and J. A. Orcutt, Distribution of magma beneath the East Pacific Rise between the Clipperton Transform and the 9°17′N deval from forward modeling of common depth point data, *J. Geophys. Res.*, *98*(B8), 13,945–13,969, 1993.

Koper, K. D., et al., Modeling the Tonga slab: Can travel time data resolve a metastable olivine wedge?, *J. Geophys. Res.*, *103*(12), 30,079–30,100, 1998.

Linville, A. F., Single-channel digital filter design for seismic applications, *Geophysics*, *59*(10), 1584–1592, 1994.

Lonsdale, P., A multibeam reconnaissance of the Tonga Trench axis and its intersection with the Louisville Guyot chain, *Mar. Geophys. Res.*, *8*, 295–327, 1986.

McLennan, S. M., and S. R. Taylor, Geochemical constraints on the growth of the continental crust, *J. Geol.*, *90*, 347–361, 1982.

Mitronovas, W., and B. Isacks, Seismic velocity anomalies in the upper mantle beneath the Tonga-Kermadec Island Arc, *J. Geophys. Res.*, *76*, 7154–7180, 1971.

Morton, J. L., and N. H. Sleep, Seismic reflections from a Lau Basin magma chamber, in *Geology and Offshore Resources of Pacific Island Arc—Tonga Region*, edited by D. W. Scholl and T. L. Vallier, pp. 441–453, Circum-Pacific Counc. for Energy and Miner. Resour., Houston, Tex., 1985.

Parson, L. M., and J. W. Hawkins, Two-stage ridge propagation and the geological history of the Lau backarc basin, *Proc. Ocean Drill. Program Sci. Results*, *135*, 819–828, 1994.

Parson, L. M., R. G. Rothwell, and C. J. Macleod, Tectonics and sedimentation in the Lau Basin (southwest Pacific), *Proc. Ocean Drill. Program Sci. Results*, *135*, 9–21, 1994.

Pontoise, B., and G. Latham, Etude par refraction de la structure interne de l'arc des Tonga, in *Contribution a l'Etude Geodynamique du Sud-Ouest Pacifique*, pp. 283–291, ORSTOM Inst., Paris, 1982.

Purdy, G. M., et al., Relationship between spreading rate and the seismic structure of mid-ocean ridges, *Nature*, *355*, 815–817, 1992.

Raitt, R. W., R. L. Fisher, and R. G. Mason, Tonga trench, *Spec. Pap. Geol. Soc. Am.*, *62*, 237–254, 1955.

Roth, E. G., et al., Seismic attenuation tomography of the Tonga-Fiji region using phase pair methods, *J. Geophys. Res.*, *104*(3), 4795–4809, 1999.

Shipboard Scientific Party, Site 834, in *Proceedings of the Ocean Drilling Program, Initial Reports*, edited by L. Parson et al., pp. 85–180, Ocean Drill. Program, College Station, Tex., 1992a.

Shipboard Scientific Party, Site 835, in *Proceedings of the Ocean Drilling Program, Initial Reports*, edited by L. Parson et al., pp. 181–236, Ocean Drill. Program, College Station, Tex., 1992b.

Sohn, R. A., et al., Three-dimensional tomographic velocity structure of upper crust, Coaxial segment, Juan de Fuca Ridge: Implications for on-axis evolution and hydrothermal circulation, *J. Geophys. Res.*, *102*(B8), 17,679–17,695, 1997.

Spudich, P., and J. Orcutt, A new look at the seismic velocity structure of the oceanic crust, *Rev. Geophys.*, *18*(3), 627–645, 1980.

Suyehiro, K., et al., Continental crust, crustal underplating, and low-Q upper mantle beneath an oceanic island arc, *Science*, *272*, 390–392, 1996.

Taylor, B., et al., Sea-floor spreading in the Lau back-arc basin, *Earth Planet. Sci. Lett.*, *144*, 35–40, 1996.

Turner, I. M., C. Peirce, and M. C. Sinha, Seismic imaging of the axial region of the Valu Fa Ridge, Lau Basin: The accretionary processes of an intermediate back-arc spreading ridge, *Geophys. J. Int.*, *138*(2), 495–519, 1999.

White, R. S., D. McKenzie, and R. K. O'Nions, Oceanic crustal thickness from seismic measurements and rare earth element inversions, *J. Geophys. Res.*, *97*(B13), 19,683–19,715, 1992.

Wright, D. J., et al., Bathymetry of the Tonga trench and forearc: A map series, *Mar. Geophys. Res.*, *21*(5), 489–512, 2000.

Xu, Y., and D. A. Wiens, Upper mantle structure of the southwest Pacific from regional waveform inversion, *J. Geophys. Res.*, *102*(12), 27,439–27,451, 1997.

Zellmer, K. E., and B. Taylor, A three-plate kinematic model for Lau Basin opening, *Geochem. Geophys. Geosyst.*, *2*, 2000GC000106, 2001.

Zelt, C. A., Modeling strategies and model assessment for wide-angle seismic traveltime data, *Geophys. J. Int.*, *139*, 183–204, 1999.

Zelt, C. A., and D. A. Forsyth, Modeling wide-angle seismic data for crustal structure: Southeastern Grenville Province, *J. Geophys. Res.*, *99*(6), 11,687–11,704, 1994.

Zelt, C. A., and R. B. Smith, Seismic traveltime inversion for 2-D crustal velocity structure, *Geophys. J. Int.*, *108*, 16–34, 1992.

Zhang, Y.-S., and T. Tanimoto, Ridges, hotspots and their interaction as observed in seismic velocity maps, *Nature*, *355*, 45–49, 1992.

Zhao, D., et al., Depth extent of the Lau back-arc spreading center and its relation to subduction processes, *Science*, *278*, 254–257, 1997.

W. C. Crawford, Laboratoire de Geosciences Marines, Institut de Physique du Globe de Paris, 4 Place Jussieu, 75252 Paris Cedex 05, France. (crawford@ipgp.jussieu.fr)

L. M. Dorman, MPL/GRD, Scripps Institution of Oceanography, University of California, San Diego, 9500 Gilman Drive, La Jolla, CA 92093-0220, USA.

J. A. Hildebrand, Scripps Institution of Oceanography, University of California, San Diego, 9500 Gilman Drive, La Jolla, CA 92093-0205, USA.

S. C. Webb, Lamont Doherty Earth Observatory, P. O. Box 100, Palisades, NY 10964, USA.

D. A. Wiens, Department of Earth and Planetary Sciences, Washington University, 1 Brookings Drive, St Louis, MO 63130-4899, USA.

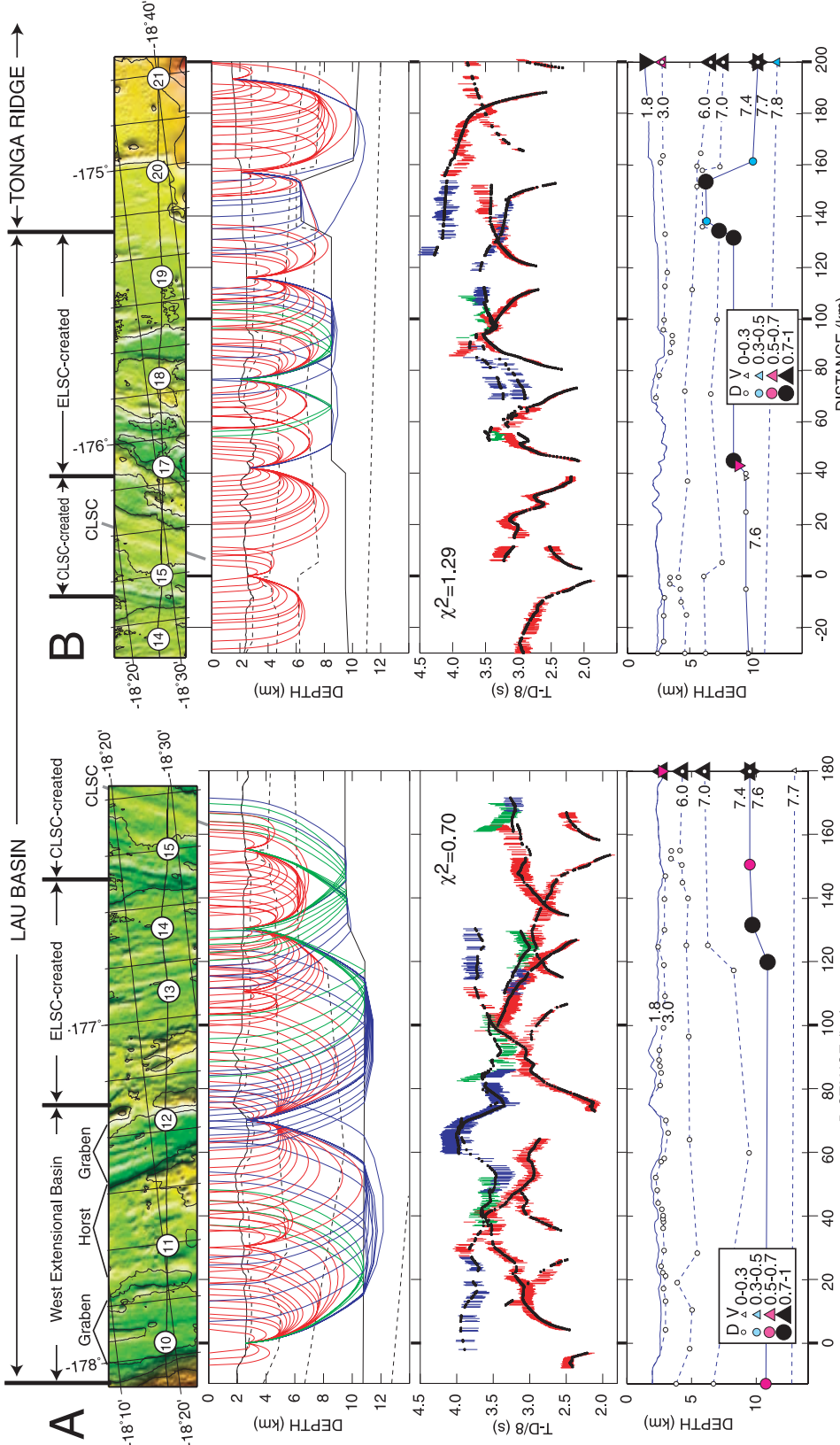

Figure 4. Preferred velocity models: (a) West Lau section, (b) East Lau section, (c) Tonga section, (d) Pacific section. The top plot shows the bathymetry [*Zellmer and Taylor*, 2001], OBS locations (circles), and the air gun line (solid line). The second plot shows ray paths (every fifth ray) and the velocity model. Dashed lines indicate layer boundaries with continuous velocities; solid lines indicate boundaries with velocity discontinuities. Colored lines trace the modeled ray paths (red = *Pg* (crust), green = *PmP* (Moho reflections), blue = *Pn* (crust-mantle)). The third plot shows the data fit, with measured travel times and their uncertainty shown in color and the modeled arrival times shown in black. The bottom plot shows uncertainty estimates calculated from the resolution matrix (larger symbols indicate better resolution): circles = depth nodes, upward pointing triangles = velocity at the bottom of the overlying layer, downward pointing triangles = velocity at the top of the underlying layer [*Zelt*, 1999]. Where there is only one type of triangle, velocity is continuous across the boundary. Constant velocity boundaries only have triangles at the right edge. If two boundaries "pinch out" together (usually at the seafloor), we moved the triangle for the upper boundary to the point of easternmost separation of the layers. In the legend, D = depth and V = velocity.

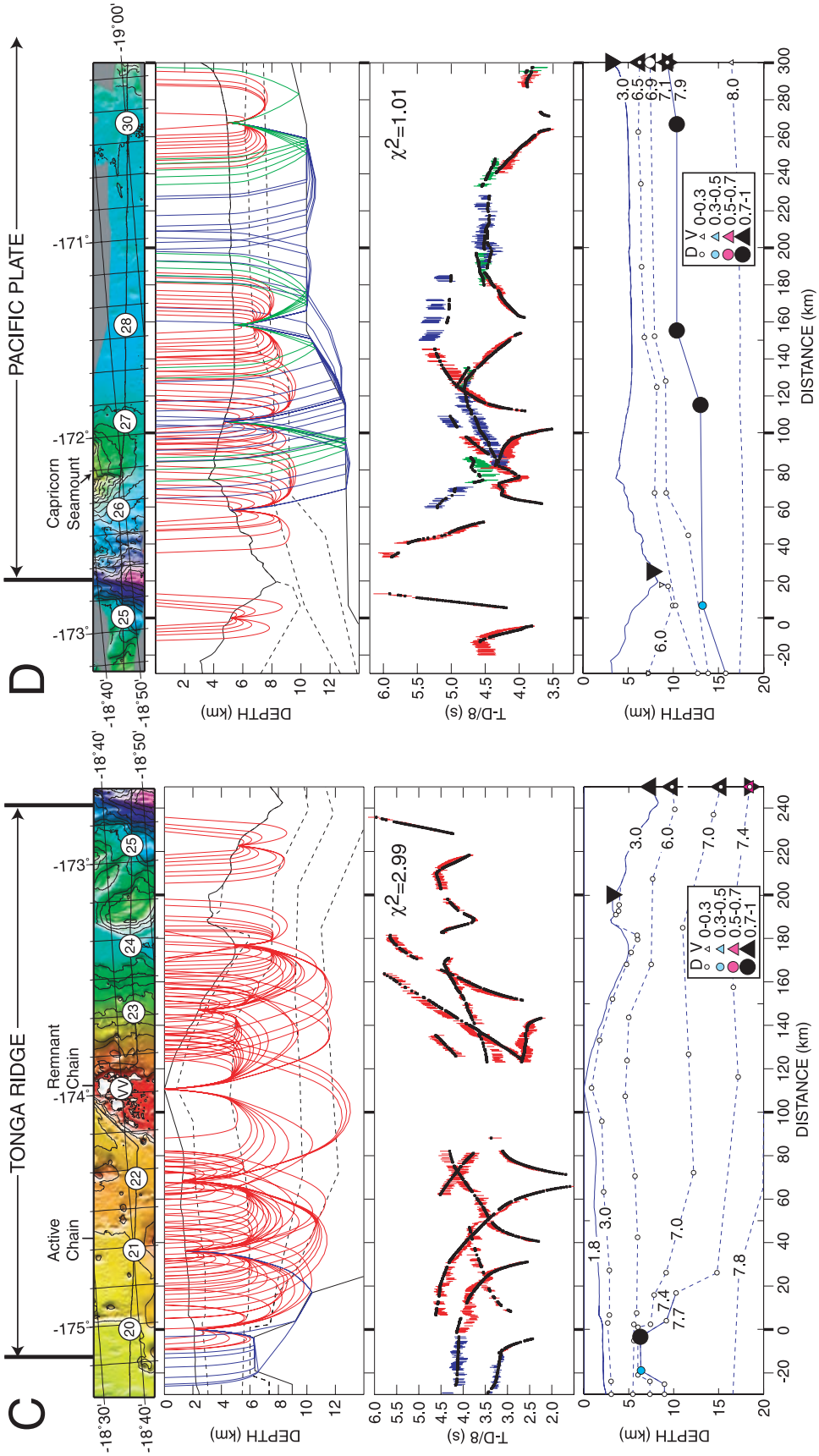

Figure 4. (continued)